An extended ab initio QM/MM MD approach to structure and dynamics of Zn(II) in aqueous solution

ARTICLE *in* THE JOURNAL OF CHEMICAL PHYSICS · SEPTEMBER 2005

Impact Factor: 2.95 · DOI: 10.1063/1.1996575 · Source: PubMed

4 AUTHORS, INCLUDING:

M. Qaiser Fatmi
COMSATS Institute of Information Technology
22 PUBLICATIONS **243** CITATIONS
SEE PROFILE

Manfredo Rode
Chulalongkorn University
205 PUBLICATIONS **4,586** CITATIONS
SEE PROFILE

An extended *ab initio* QM/MM MD approach to structure and dynamics of Zn(II) in aqueous solution

M. Qaiser Fatmi, Thomas S. Hofer, Bernhard R. Randolf, and Bernd M. Rode[a)]
Theoretical Chemistry Division, Institute of General, Inorganic and Theoretical Chemistry, University of Innsbruck, Innrain 52a, A-6020 Innsbruck, Austria

(Received 11 May 2005; accepted 16 June 2005; published online 10 August 2005)

Structural and dynamical properties of Zn(II) in aqueous solution were investigated, based on an *ab initio* quantum mechanical/molecular mechanical (QM/MM) molecular dynamics simulation at double-ζ Hartree–Fock quantum mechanical level including the first and second hydration shells into the QM region. The inclusion of the second shell in the QM region resulted in significant changes in the properties of the hydrate. The first shell coordination number was found to be 6, the second shell consists of ~14 water molecules. The structural properties were determined in terms of RDF, ADF, tilt and theta angle distributions, while dynamics were characterized by mean ligand residence times, ion-ligand stretching frequencies and the vibrational and librational motions of water ligands. © *2005 American Institute of Physics*. [DOI: 10.1063/1.1996575]

I. INTRODUCTION

Zinc is a micro mineral in the human body which is essential for growth and development, and it acts as a cofactor for about 300 enzymes from all six enzyme classes.[1,2] It also performs uniquely as a Lewis acid catalyst in all life processes.[3] Furthermore, zinc is one of the most important basic materials in various industrial processes. Zinc offers one to seven coordination sites; in most complexes the coordination number is 4 or 6, in tetrahedral or octahedral arrangements.[4,5] Both experimental and theoretical studies have shown the primary hydration number of Zn^{2+} in dilute aqueous solution to be 6, forming an octahedral geometry.[6–13] Salmon *et al.*[14] investigated the dynamics of the zinc hydrate in $Zn(ClO_4)_2$ (1.98 and 2.58 mol kg^{-1}) and $ZnCl_2$ (1.96 mol kg^{-1}) solution by means of incoherent quasi-elastic neutron scattering (IQENS). They reported a range for the first shell ligand exchange rate from 5×10^9 s^{-1} to 10^{10} s^{-1} which refers to an intermediate exchange.

Simulation methods such as Monte Carlo (MC) and molecular dynamics (MD) have proven to be a suitable alternative to experiments for a quantitative description of physical and chemical phenomena of metal solvation, if the quantum mechanical/molecular mechanical (QM/MM) approach is employed.[15] In the present work, two QM/MM-MD simulations were performed in order to evaluate the structural and dynamical properties of the Zn(II)-water complex. The results obtained after inclusion of the second shell in the QM region showed a modification of structure and dynamics of the zinc hydrate compared to the one-shell QM/MM-MD simulation, apparently due to the importance of many body quantum effects also in the second shell.

[a)]Author to whom correspondence should be addressed. Telephone: +43-512-507-5160. Fax: +43-512-507-2714. Electronic mail: bernd.m.rode@uibk.ac.at

II. METHODOLOGY

A. Construction of potential functions

The first step of a QM/MM-MD simulation is the choice of a proper basis set and the level of theory applied in the QM region. In recent investigations it has been found that Dunning DZP basis sets for oxygen and hydrogen can be successfully applied,[16] so these basis sets were chosen for this investigation as well. The LANL2DZ ECP basis set for Zn(II)[17] was chosen as it includes a relativistically corrected ECP and showed no artificial charge transfer by scanning the $Zn-H_2O$ hypersurface. The same basis set has already been used by Mohammed *et al.*[13] and Pavlov *et al.*[18]

In order to gain more information about the $Zn-H_2O$ system, geometry optimizations of $[Zn(H_2O)_n]^{2+}$ clusters ($n=1-4,6$) were carried out at different levels of theory, namely HF, B3LYP, MP2, MP4-SDQ, CCSD and QCISD (Tables I and II). The bond distances (Table I) for all methods and cluster sizes are identical, varying ±0.01 Å, thus showing a minor influence of electron correlation on the $Zn-H_2O$ geometry.

With regard to the average binding energy, ΔE_{bond} (Table II), the influence of correlation is higher. The correlated methods show almost identical values within 0.5 kcal/mol, the deviation becoming smaller with increasing cluster size.

TABLE I. Average binding energies in kcal/mol for $[Zn(H_2O)_n]^{2+}$ clusters, obtained from HF, CCSD, QCISD, MP4-SDQ, MP2 and B3LYP calculations.

	E_{bond} in kcal/mol					
n	HF	MP4-SDQ	CCSD	QCISD	MP2	B3-LYP
1	−88.3	−92.0	−91.5	−91.8	−92.6	−98.3
2	−83.7	−87.3	−86.8	−87.1	−87.8	−91.9
3	−75.1	−78.2	−77.9	−78.0	−78.7	−82.0
4	−68.0	−71.0	−70.7	−70.9	−71.4	−74.0
6	−53.7	−56.6	−56.4	−56.5	−57.0	−58.3

TABLE II. Average Zn–O distances in Å for $[Zn(H_2O)_n]^{2+}$ clusters obtained from HF, CCSD, MP4-SDQ, QCISD, MP2 and B3LYP calculations.

	r_{Zn-O} in Å					
n	HF	MP4-SDQ	CCSD	QCISD	MP2	B3-LYP
1	1.90	1.90	1.90	1.90	1.90	1.90
2	1.91	1.90	1.90	1.90	1.90	1.91
3	1.97	1.97	1.97	1.97	1.97	1.97
4	2.02	2.02	2.02	2.02	2.02	2.02
6	2.16	2.15	2.15	2.15	2.15	2.15

The deviation of Hartree–Fock (HF) and B3LYP energies for the monohydrate is −3.5 and +6.5 kcal/mol, respectively, the deviation being reduced again with increasing size of the cluster. An estimation of the basis set superposition error for the zinc monohydrate was carried out (Table III). It can be seen that the BSSE of B3LYP is considerably higher whereas the other methods yield an identical value, amounting to ~2% of the computed binding energies.

Based on these data the *ab initio* HF method was to be preferred for our simulations as correlated methods are too demanding in terms of computational time and the hybride DFT approach showed a stronger deviation from the correlated methods than *ab initio* HF SCF.

In order to describe the MM interactions between the species in the system a new two-body interaction potential was constructed from more than 7000 *ab initio* energy points calculated at restricted Hartree–Fock (RHF) level using the LANL2DZ ECP basis set for Zn^{2+} and double-ζ plus polarization basis sets for oxygen and hydrogen.[16] The TURBOMOLE 5.5 (Refs. 19–22) program was used to compute the two-body energies using the following formula:

$$\Delta E^{2bd} = E^{ab}_{MW} - (E^{ab}_{M} + E^{ab}_{W}), \tag{1}$$

where E^{ab}_{MW} is the *ab initio* energy of the $Zn-H_2O$ structure, E^{ab}_{M} and E^{ab}_{W} represent the *ab initio* energies of zinc(II) and water, respectively. Throughout the whole calculation, the geometry of water was kept constant at its experimental gas phase values[23] ($O-H=0.9601$ Å, $H-O-H=104.47°$). This energy hypersurface was fitted to an analytical two-body function [Eq. (2)] using the Levenberg–Marquardt algorithm; the partial charges of oxygen and hydrogen were set to −0.6598 and 0.3299, respectively, according to the BJH–CF2 water model[24–26] employed in this simulation:

$$\Delta E^{2bd}_{Fit} = \frac{q_{Zn^{2+}}q_O}{r} + \frac{A_O}{r^5} + \frac{B_O}{r^6} + \frac{C_O}{r^{10}} + \frac{D_O}{r^{12}} + \sum_{i=1}^{2}\left(\frac{q_{Zn^{2+}}q_H}{r_i} + \frac{A_H}{r_i^5} + \frac{B_H}{r_i^7} + \frac{C_H}{r_i^{11}} + \frac{D_H}{r_i^{12}}\right), \tag{2}$$

A, *B*, *C* and *D* are the fitting parameters (Table IV), $q_{Zn^{2+}}$, q_O and q_H are the charges of zinc, oxygen and hydrogen, respectively, and *r* and r_i are the distances Zn–O and Zn–H, respectively. The lowest energy for the Zn(II)-water interaction was found to be −88.4 kcal/mol at a distance of 1.91 Å, the root mean square deviation (rmsd) of the fitted function is 2.3 kcal/mol.

TABLE III. Basis set superposition error according to Boys–Bernardi procedure for $Zn(II)-H_2O$ obtained from HF, CCSD, QCISD, MP4-SDQ, MP2 and B3LYP calculations.

BSSE in kcal/mol					
HF	CCSD	QCISD	MP4–SDQ	MP2	B3–LYP
1.7	1.7	1.7	1.7	1.7	2.9

TABLE IV. Optimized parameters for the Zn–O and Zn–H two-body interactions.

	Parameters in kcal/mol			
	A	*B*	*C*	*D*
Zn–O	−9519.05	19094.37	−34732.56	32684.47
Zn–H	−1156.34	6116.94	−50493.35	50951.42

As pair potentials are not sufficient to correctly evaluate all the properties of strongly hydrated ions,[27–32] a three-body correction potential was constructed. More than 15 000 *ab initio* energies were computed as follows:

$$\Delta E^{3bd}_{corr} = E^{ab}_{WMW} - \left(E^{ab}_{M} + \sum_{W=1}^{2} E^{ab}_{W}\right) - \sum_{W=1}^{2} E^{2bd}_{MW} - E^{2bd}_{WW}, \tag{3}$$

where E^{ab}_{WMW}, E^{ab}_{M} and E^{ab}_{W} are the SCF energies of $[Zn(H_2O)_2]^{2+}$, Zn(II) and water, respectively. E^{2bd}_{MW} is the energy of $Zn-H_2O$ obtained from the pair potential [Eq. (2)] and E^{2bd}_{WW} denotes for the water–water interaction according to the BJH–CF2 (Refs. 24 and 25) water model. The obtained three-body correction function is

$$\Delta E^{3bd}_{Fit} = 0.64 \exp^{-0.23(r_1+r_2)} \exp^{-0.48r_3}(CL-r_1)^2(CL-r_2)^2, \tag{4}$$

where r_1 and r_2 are the distances $Zn-O_1$ and $Zn-O_2$, respectively, r_3 is the distance between O_1 and O_2. CL is a cutoff limit set to 6.0 Å, where three-body terms become negligible.

B. Simulation protocol

For the classical MD simulation a cubic box with a side length 24.71 Å containing one Zn(II) and 499 water molecules was used, corresponding to a density of the system as of the pure solvent at 298 K (0.99702 g/cm^3).[33] A canonical NVT ensemble was used employing periodic boundary condition, and the temperature was kept constant at 298.16 K using the Berendsen algorithm[34,35] with a relaxation time of 0.1 ps. The cutoff distances were set to 5.0 Å for O–H and 3.0 Å for H–H non-Coulombic interactions. For all other pair interactions the cutoff was set to 12.35 Å. In order to account for the long-range electrostatic interactions, the reaction field method was employed.[36] The flexible BJH–CF2 water model[24,25] was used, which includes an intramolecular potential enabling explicit hydrogen movements. Therefore, the time step for the simulation was set to 0.2 fs. A classical MD simulation was performed for 20 ps (after 10 ps of equilibration) using the two-body potential. After inclusion of the three-body correction potential and 10 ps re-equilibration further 250 ps were sampled.

The one-shell QM/MM-MD simulation was started from an equilibrated configuration of the classical three-body corrected simulation. The diameter of the QM sphere was set to 6.8 Å in accordance with the Zn–O radial distribution function (RDF) obtained from the classical simulation. Similarly, the two-shell QM/MM simulation was started from an equilibrated geometry of the one-shell simulation, setting the diameter of the QM region to 10.0 Å according to the Zn–O RDF obtained from the one-shell simulation. This extension increases the computational effort by a factor of ~80. After 2 ps of re-equilibration the one- and two-shell QM/MM-MD simulations were performed for 15 and 12 ps, respectively. The total force acting on a particle is calculated according to the following expression:

$$F_{\mathrm{tot}} = F_{MM}^{sys} + S(r) * (F_{QM}^{QM} - F_{QM}^{MM}), \tag{5}$$

where F_{tot} is the total force acting on a particle, F_{MM}^{sys} is the MM force of the whole system and F_{QM}^{QM} and F_{QM}^{MM} are QM and MM forces in QM region. A smoothing function $S(r)$ is applied in a region of 0.2 Å to ensure a smooth transition of water molecules[32] between the QM and MM regions:

$$S(r) = 0, \quad \text{for } r \leqslant r_1,$$

$$S(r) = \frac{(r_0^2 - r^2)^2 (r_0^2 + 2r^2 - 3r_1^2)}{(r_0^2 - r_1^2)^3}, \quad \text{for } r_1 < r \leqslant r_0,$$

$$S(r) = 1, \quad \text{for } r > r_0. \tag{6}$$

Radial and angular distribution functions were employed to characterize the structural properties of zinc in aqueous solution. The evaluation of librational and vibrational properties of water was carried out using velocity autocorrelation functions (VACFs), $C(t)$, defined as

$$C(t) = \frac{\sum_i^{N_t} \sum_j^N \vec{v_j}(t_i)\vec{v_j}(t_i + t)}{N_t N \sum_i^{N_t} \sum_j^N \vec{v_j}(t_i)\vec{v_j}(t_i)}, \tag{7}$$

where N is the number of particles, N_t is the number of time origins t_i, and $\vec{v_j}$ denotes a given velocity component of the particle j. The power spectrum of the VACF was calculated by Fourier transformation, using a correlation length of 2.0 ps with 2000 averaged time origins. Librational and vibrational frequencies of water molecules and ion–oxygen stretching frequencies were computed using the approximative normal coordinate analysis.[37]

Mean ligand residence times (MRT, τ) in first and second hydration shell were calculated using the direct method.[38] The parameter t^*, determining the minimum time span to account a ligand displacement from its original shell, was set to 0 and 0.5 ps, respectively. The sustainability of exchange processes can be defined as

$$S_{ex} = \frac{N_{ex}^{0.5}}{N_{ex}^{0}}, \tag{8}$$

where S_{ex} is the sustainability coefficient, N_{ex}^0 is the number of all transitions through a shell boundary ($t^*=0$), and $N_{ex}^{0.5}$ denotes the number of exchanges persisting longer than 0.5 ps. Its inverse $(1/S_{ex})$ accounts how many attempts are needed to produce one lasting exchange between the hydration shells and/or bulk. Reorientational time correlation function (RTCFs) of water molecules were calculated as

$$C_{li}(t) = \langle P_l[\vec{u_i}(0)\vec{u_i}(t)] \rangle, \tag{9}$$

where P_l is the Legendre polynomial of lth order and $\vec{u_i}$ is a unit vector along the three principal axes i defined in a fixed coordinate frame. The RTCFs were fitted to the following simple form:

$$C_l(t) = a \exp(-t/\tau_1), \tag{10}$$

where a and τ_1 are the fitting parameters and τ_1 corresponds to the relaxation time.

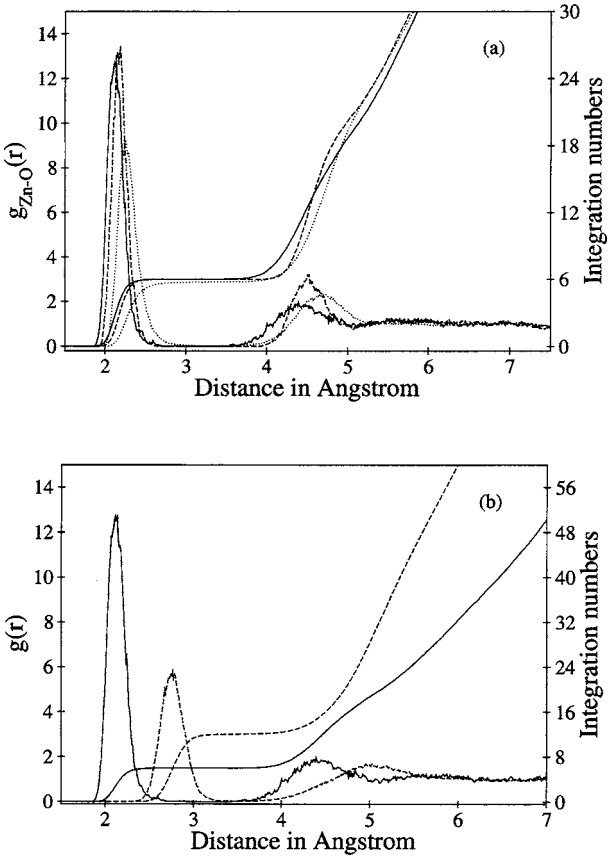

FIG. 1. (a) Zn–O RDFs obtained from the two-shell QM/MM (solid line), the one-shell QM/MM (dashed line) and the classical MD (dotted line) simulations and (b) Zn–O (solid line) and Zn–H (dashed line) RDFs and their running integration numbers obtained from the two-shell QM/MM-MD.

III. RESULTS AND DISCUSSION

A. Structural properties

The radial distribution functions (RDFs) of Zn^{2+} together with their running integration numbers, obtained from the classical and both QM/MM-MD simulations are displayed in Fig. 1(a), the main structural parameters are listed in Table V. Two well-defined peaks are observed in all three RDFs, indicating the formation of distinct first and second hydration shells. A third shell cannot be distinguished from the bulk. The peak maxima of the first and second shell in the Zn^{2+}–O RDF obtained from the two-shell QM/MM-MD

TABLE V. Characteristic values of radial distribution functions $g_{Zn-O}(r)$ and $g_{Zn-H}(r)$ for Zn^{2+} in aqueous solution obtained from one- and two-shell QM/MM and classical molecular dynamic simulations. r_M denotes maxima and r_M minima observed in the RDFs.

Method	r_{M1} (Å)	r_{m1} (Å)	$CN_{av,1}$	r_{M2} (Å)	r_{m2} (Å)	$CN_{av,2}$
			Zn–O			
Classical	2.24	3.33	5.8	4.73	5.60	21.0
1-shell QM/MM	2.18	2.70	6.0	4.50	5.06	14.7
2-shell QM/MM	2.11	2.91	6.0	4.40	5.11	13.8
			Zn–H			
Classical	2.99/3.01	3.76	11.5	5.22	6.35	60.2
1-shell QM/MM	2.82	3.52	12.0	5.10	5.96	50.6
2-shell QM/MM	2.76	3.55	12.0	5.03	6.18	53.6

simulation appeared at the closer distances of 2.11 and 4.40 Å, respectively, compared to the one-shell QM/MM and classical MD simulations. Apparently the inclusion of *n*-body and polarization effects in the second shell and the better description of the hydrogen bonds between first and second shell due to the quantum mechanical treatment, has an essential influence, as only this result is in perfect agreement with the experimental results ranging from 2.09–2.13 Å obtained from ND, XRD and EXAFS measurements.[39–46] The high intensity of the first shell peaks shows stability and rigidity of the zinc hydrate. However, shoulders are recognizable at the tip of the peak, reflecting slightly different bond lengths. Unlike in the classical simulations, the first solvation shell in both QM/MM-MD simulations is completely separated from the second shell, showing no exchange process between these shells within the simulation time. However, the peaks in the two-shell QM/MM-MD simulation are broader than in the one-shell QM/MM-MD, indicating more flexibility of the structure.

Figure 1(b) shows the Zn–O and Zn–H radial distribution functions obtained from the two-shell QM/MM-MD simulation. The Zn–O and Zn–H peaks are not overlapping, thus suggesting a rather rigid orientation of the water dipole vector, whereas the orientation is more freely in the second hydration shell. Compared to the results obtained from an extended QM/MM-MD simulation for Al(III),[47] which is even more polarizing, the second shell is rather mobile.

The coordination number distributions of hydrated Zn^{2+} obtained from the QM/MM and classical molecular dynamic simulations are shown in Fig. 2. Contrary to the classical simulation, both QM/MM-MD simulations showed a sixfold coordination with 100% occurrence, which is in good agreement with experimental values (6) (Refs. 11, 39–43, and 46) and theoretical studies obtained from *ab initio* MO calculations (6) (Refs. 13 and 48) and MC simulations (5.6).[49] In the classical simulation fivefold coordination was also observed along with the sixfold one, occurring to about 26%. The coordination number of the second hydration shell ranges from 10–18 with a maximum of 14 for the two-shell QM/MM-MD simulation. In the one-shell simulation it varies from 11–19, the highest probability being 15 while the classical simulation strongly overestimates the second shell coordination number, predicting 21 as the most probable one in a much broader distribution.

Figure 3 displays the angular distribution functions of $O-Zn^{2+}-O$ obtained from all three simulations. In all cases two peaks located at ~90° and ~173° are shown, as already obtained from the classical MD simulations by Obst *et al.*,[10] and indicating an almost perfect octahedral arrangement of the $[Zn(H_2O)_6]^{2+}$ species (Fig. 4). The peaks from the two-shell simulation are broader and less intense than those of the one-shell QM/MM simulation, further pointing toward a more flexible structure.

In order to describe the orientation of water molecules relative to the ion two angles were defined: θ as the angle

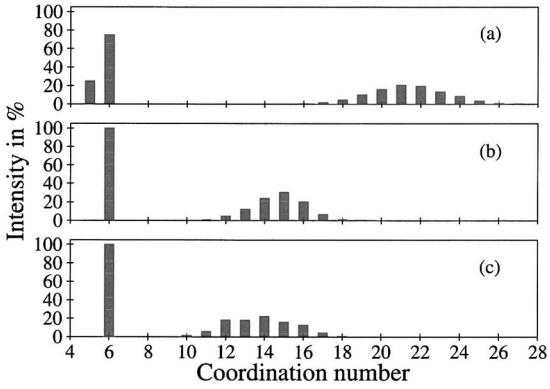

FIG. 2. Coordination number distributions of first and second shell of hydrated Zn(II) obtained from (a) the classical, (b) the one-shell QM/MM and (c) the two-shell QM/MM-MD simulations.

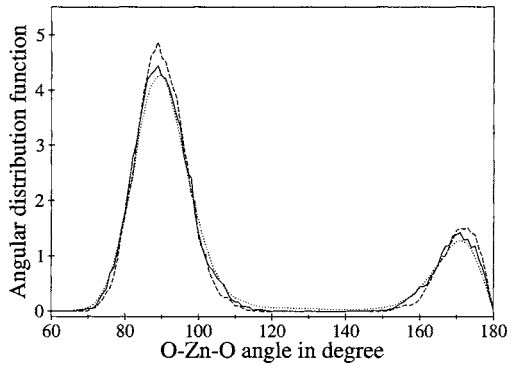

FIG. 3. Angular distributions of the O–Zn(II)–O angle in degrees obtained from the two-shell QM/MM (solid line), the one-shell QM/MM (dashed line) and the classical (dotted line) MD simulation.

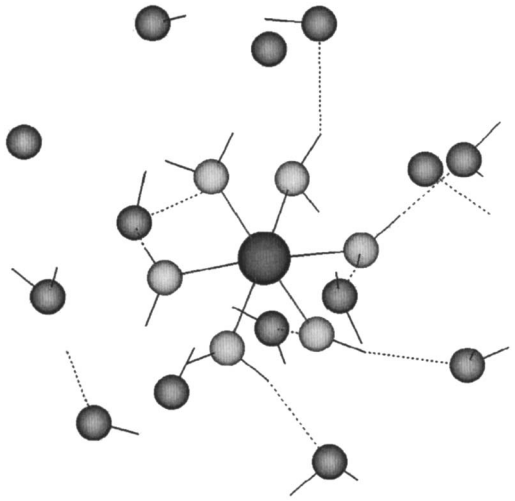

FIG. 4. Octahedral structure of the Zn–water complex in the first hydration shell (snapshot taken by MOLVISION).

between Zn–O vector and the dipole vector, and "tilt" as the angle between Zn–O connection vector and the plane formed by the O–H vector. The tilt and θ angle distributions of the first shell for all three simulations are displayed in Fig. 5.

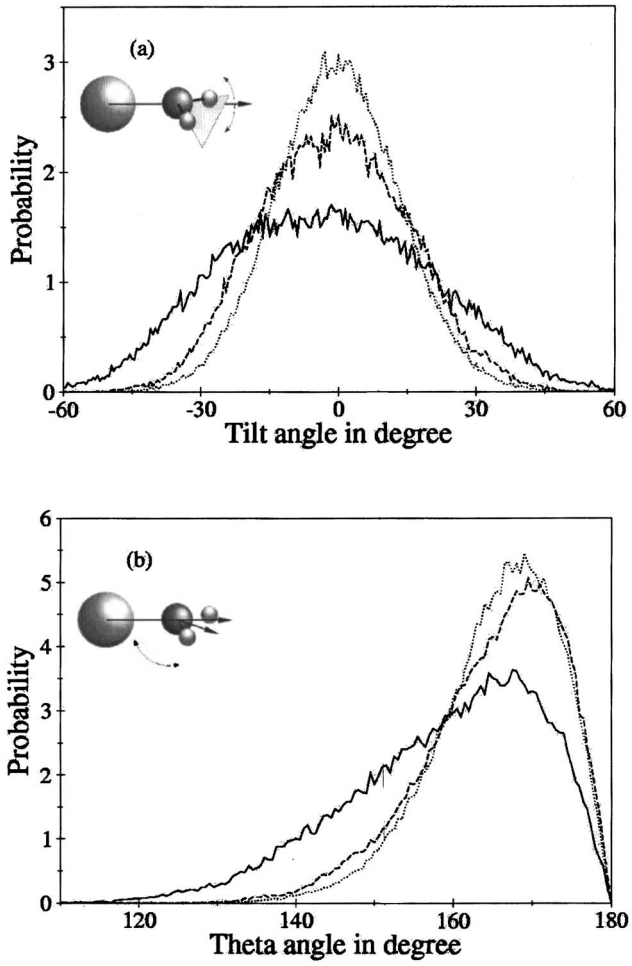

FIG. 5. Tilt and theta angle distributions of the Zn(II)–water geometry obtained from the two-shell QM/MM (solid line), the one-shell QM/MM (dashed line) and the classical (dotted line) MD simulations.

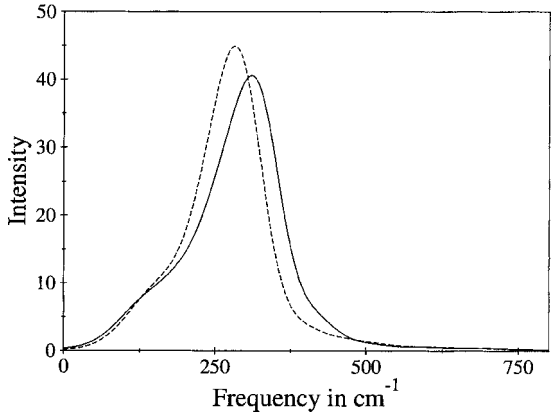

FIG. 6. Power spectra of the Zn–O stretching frequency in cm^{-1} obtained from the two-shell QM/MM (solid line) and the one-shell QM/MM (dashed line) MD simulations.

The higher flexibility of the zinc(II)-water complex in the case of the two-shell QM/MM-MD simulation is clearly visible. The tilt angle distribution gets broader with increasing radius of the quantum mechanical subsystem as already observed in a two-shell QM/MM-MD simulation of Al(III).[47] The same is true in the case of the θ angle distribution. In contrast to the results of θ angle obtained by Mohammed *et al.*[13] the maxima of the θ angle distribution of the first shell are observed at $\sim 169°$ in both classical and QM/MM-MD simulation. The degree of flexibility increases with increasing QM radius, and in the two-shell QM/MM-MD simulation a noticeable tailing toward lower angles is observed. As to be expected, both tilt and θ angle distributions show more flexibility of the first shell than in the case of Al(III).[47]

B. Dynamical properties

Figure 6 displays the power spectrum of the Zn–O stretching vibration, obtained from both one- and two-shell QM/MM-MD simulations. The frequencies were scaled by the standard factor of 0.89.[50,51] The peak maximum from the two-shell QM/MM-MD simulation (310 cm^{-1}; force constant 73 Nm^{-1}) is found at a considerably higher frequency than that from the one-shell QM/MM-MD simulation (282 cm^{-1}; force constant 60 Nm^{-1}), which reflects an improved description of ion-ligand bonding by inclusion of the second hydration shell in the QM region. A shoulder is visible at lower frequencies in the peaks of both QM/MM-MD simulations thus strongly suggesting the presence of nonequivalent Zn–O bonds.

The power spectra of the velocity autocorrelation functions (VACFs) for the librational motions of water molecules around the principle axes R_x, R_y and R_z and the vibrational motions for bond stretching (Q_1 and Q_3) and bending (Q_2) obtained from the two-shell QM/MM-MD simulation are shown in Fig. 7, the frequencies for both QM/MM-MD simulations are summarized in Table VI. The frequencies of the water molecules located in the QM region were scaled by a standard factor of 0.89.[50,51] The order of librational motions of water in the first hydration shell of the one-shell QM/MM-MD simulation is $R_x > R_y > R_z$, in agreement with the results previously reported by Mohammed *et al.*[13] How-

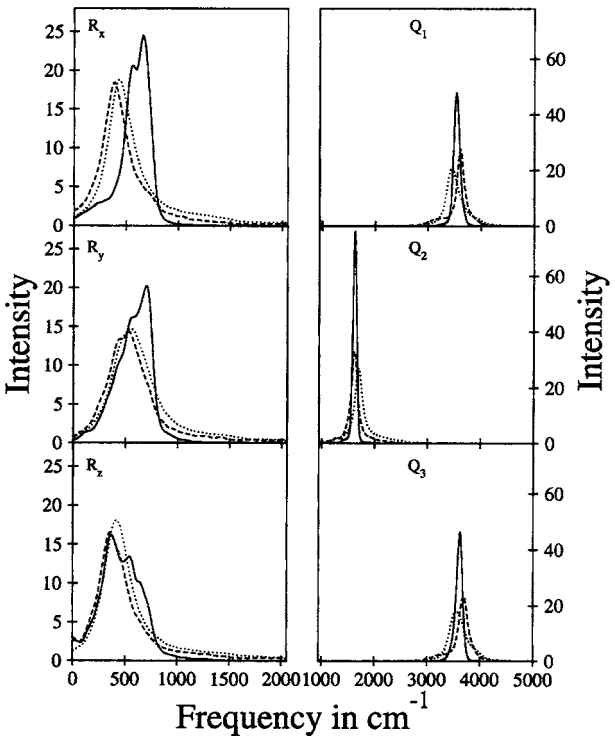

FIG. 7. Power spectra of librational and vibrational modes for water in cm^{-1} obtained from the two-shell QM/MM simulations in the first (solid line) and the second hydration shell (dashed line) and the bulk (dotted line).

ever, the order in the second shell for both QM/MM-MD simulations is $R_y > R_x > R_z$ as already obtained for other ions.[15,52–54] In the two-shell QM/MM-MD simulation the split peaks further strengthen the assumption of nonequivalent Zn(II)-water bonds. This splitting is not observed in the one-shell QM/MM-MD simulation, where only some shoulders appear. In the first shell of both QM/MM simulations the rotational frequencies around x and y axes and the symmetric (Q_1) and antisymmetric (Q_3) stretching frequencies are blue-shifted while the bending frequencies (Q_2) are red-shifted with respect to the bulk. Contrary to the one-shell QM/MM-MD simulation, the second shell stretching frequencies (Q_1 and Q_3) of the two-shell simulation are blue-shifted, reflecting a shorter distance between zinc and water

TABLE VII. Reorientational times (τ) of first and second order of water molecules in the first and second shell and the bulk of Zn(II) obtained from the two-shell QM/MM-MD simulation of Zn(II) in aqueous solution.

	Reorientational time in ps					
Phase	τ_{1x}	τ_{1y}	τ_{1z}	τ_{2x}	τ_{2y}	τ_{2z}
1st shell	3.7	17	3.4	2.6	5.8	1.9
2nd shell	3.1	3.7	2.3	1.6	1.3	1.0
Bulk	7.4	7.4	4.9	3.6	3.1	2.6
H_2O(exp.)[a]		7.5			2.5	

[a]Experimental reorientational correlation time of water (Ref. 60).

while the bending (Q_2) and librational frequencies around the x and z axes are red-shifted compared to the bulk, showing more flexibility of water ligands in this shell. This contradiction in the frequencies makes it mandatory to extend the QM radius up to the second shell for a correct evaluation of dynamics.

Table VII refers the first- and second-order reorientational times for water molecules around the x, y and z axes in the first and second shell and in the bulk, obtained from the two-shell QM/MM-MD simulation. In both QM/MM-MD simulations the first shell shows the highest relaxation time for rotations around the y axis and consequently this is the most hindered rotation. However, all the values are much higher in the one-shell QM/MM-MD simulation compared to the two-shell approach. These findings reveal that the influence of polarization and many-body quantum effects are important to obtain a correct description of the dynamical properties of water ligands in the zinc hydrate.

Zn(II)-water distance plots obtained from the two-shell QM/MM and the classical MD simulations are depicted in Fig. 8. The number of exchanges per 10 ps and the mean ligand residence time obtained from the QM/MM and the classical MD simulations are summarized in Table VIII. As to be expected, both QM/MM-MD simulations did not show any exchange events in the first shell during the simulation time. However, in contrast to the classical MD simulation performed by Mohammed *et al.*,[13] 48 exchange processes were observed during our classical simulation time of

TABLE VI. Librational and vibrational frequencies in cm^{-1} of water molecules in the first and second hydration shell and the bulk of Zn(II) ion in aqueous solution.

		R_x	R_y	R_z	$Q1$	Q_2	Q_3
1-shell QM/MM	1st shell[a]	630	575	410	3550	1630	3620
	2nd shell	440	530	430	3450	1700	3535
	Bulk	420	540	510	3450	1700	3560
2-shell QM/MM	1st shell[a]	660,560	700,560	365,540	3540	1620	3630
	2nd shell[a]	380	530,445	360	3610	1620	3700
	Bulk	430	550	420	3450	1700	3550
Liquid[b]					3345	1645	3445
Gas[c]					3657	1595	3756
Gas[d]					3641	1601	3756

[a]Values scaled by a factor of 0.89 (Refs. 50 and 51).
[b]Experimental values in liquid water (Ref. 57).
[c]Experimental values in gas phase (Ref. 58).
[d]Scaled gas-phase vibrational frequencies using DZP basis set for water (Ref. 59).

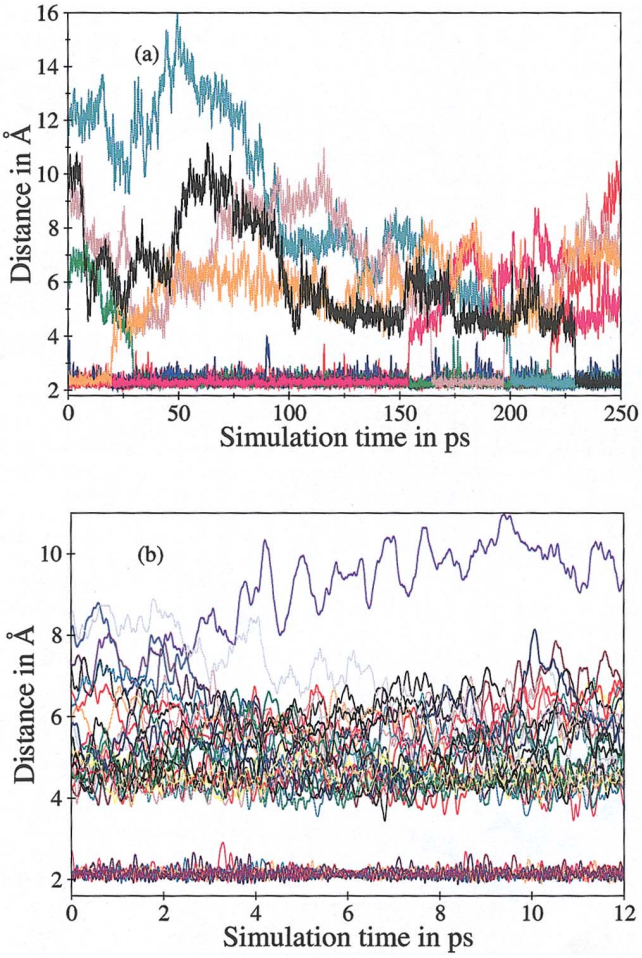

FIG. 8. (Color). Ligand exchange processes obtained from (a) the classical and (b) the two-shell QM/MM molecular dynamic simulations.

250 ps. Ten of these exchange events lasted longer than 0.5 ps, thus predicting a standardized (t^*=0.5 ps) mean residence time of 146 ps, which suggests that the mean residence time (MRT) of Zn(II) lies in the sub-nanosecond range. This result coincides well with the upper limit of the experimental estimations of Salmon *et al.*,[14] who gave lower/upper MRT limits of 0.1 and 5 ns. Table VIII also lists the sustainability of migration processes between second shell and bulk, S_{ex}, and the number of attempts needed for one successful exchange process, $1/S_{ex}$. In the two-shell QM/MM simulation approximately nine attempts are required for one real exchange process which is significantly lower than the values from the one-shell QM/MM (approximately 22) and classical (approximately 13) MD simulation. These values show that the extension of the QM treatment to the second shell increases the ligand migration rate in the second shell by a factor of ~1.5 and ~2.5 compared to the classical and one-shell QM/MM-MD simulations, respectively. The second shell ligands' MRT in the two-shell QM/MM-MD simulation was found to be 3.3 ps, which is remarkably lower than the value produced by the one-shell QM/MM-MD simulation, namely 10.5 ps, clearly proving that quantum effects are relevant for the second shell as well, when sensitive parameters like dynamical quantities are to be evaluated.

IV. CONCLUSION

From the methodical point of view this investigation showed that a two-shell quantum mechanical treatment results in significant improvements in the description of structure and especially dynamics of a hydrated ion, by its better description of hydrogen bonds between first and second shell, and the inclusion of many body quantum and polarization effects for this shell. It should be mentioned, however, that the associated computational effort is by a factor of ~80 larger than for a one-shell QM/MM simulation but this effort seems to be justified in the case of Zn(II) by the significant improvements compared to ours and previous[13] one-shell QM/MM simulations. In agreement with most experimental data a stable $[Zn(H_2O)_6]^{2+}$ complex with a Zn–O distance of 2.1 Å was observed, whose second shell consists on average of 14 ligands. The estimation of the first-shell mean ligand residence time obtained from the classical MD simulation results as ~0.15 ns. The second-shell MRT resulting as 3.3 ps, indicates high mobility of these ligands, and can be

TABLE VIII. Mean ligand residence time (τ) for t^* values of 0 and 0.5 ps, number of accounted ligand exchange events N, sustainability of migration processes to/from the first and second hydration shell S_{ex} obtained from QM/MM and classical MD simulations.

		1st shell					
		t^*=0.0 ps		t^*=0.5 ps			
System	Method	N_{ex}/10 ps	τ	N_{ex}/10 ps	τ	S_{ex}	$1/S_{ex}$
H_2O[a]	2-shell QM/MM	129	0.3	28	1.5	0.21	4.6
Zn-water	Classical	1.92	30.5	0.4	146.3	0.2	4.8
		2nd shell					
Zn-water	Classical	453	0.46	35.4	5.93	0.07	12.77
	1-shell QM/MM	306	0.4	14	10.5	0.04	21.8
	2-shell QM/MM	360	0.38	41.6	3.30	0.115	8.66

[a]MRTs and number of exchange events obtained from the two-shell QM/MM-MD simulation of pure water (Ref. 56).

compared to the corresponding values of other ions such as Cu(II)[55] (3.0 ps), Al(III)[55] (26.4 ps), Ti(III)[55] (37.0 ps) and pure water[56] (1.7 ps). From these data Zn(II) may be characterized as a structure forming ion which shows a considerable degree of polarization that influences the dynamics and ligand flexibility in the second shell. The first shell forms a stable octahedron which is kinetically inert to exchange process but shows a considerable degree of flexibility toward distortion of its octahedral geometry, especially concerning bond lengths.

ACKNOWLEDGMENTS

Financial support for this work by Austrian Science Foundation (FWF) (project P16221-N08) and a Technology Grant (BMBWK) (RFTE) for M.Q.F. are gratefully acknowledged.

[1] L. A. Gaither and J. E. David, BioMetals **14**, 251 (2001).
[2] W. Maret, BioMetals **14**, 187 (2001).
[3] T. E. Tuormaa, J. Orthomol. Med. **10**, 149 (1995).
[4] J. Burgess, *Comprehensive Coordination Chemistry* (Pergamon, Oxford, 1987), Vol. 2.
[5] F. A. Cotton and G. Wilkinson, *Advanced Inorganic Chemistry*, 5th ed. (Wiley-Interscience, New York, 1988).
[6] H. Ohtaki, T. Yamaguchi, and M. Maeda, Bull. Chem. Soc. Jpn. **49**, 701 (1976).
[7] S. P. Dagnall, D. N. Hague, and A. D. C. Towl, J. Chem. Soc., Faraday Trans. 1 **78**, 2161 (1982).
[8] B. Borzecka, S. F. Sagnowski, and S. Hodorowicz, Phys. Status Solidi A **64**, 557 (1981).
[9] W. M. Gerhard, R. T. Norbert, and M. R. Bernd, J. Phys. Chem. **100**, 6808 (1996).
[10] S. Obst and H. Bradaczek, J. Mol. Model. **3**, 224 (1997).
[11] A. Kuzmin, S. Obst, and J. Purans, J. Phys.: Condens. Matter **9**, 10065 (1997).
[12] G. Chillemi, D. A. Paola, N. V. Pavel, N. Sanna, and V. Barone, J. Am. Chem. Soc. **124**, 1968 (2002).
[13] A. M. Mohammed, H. H. Loeffler, Y. Inada, K. Tanada, and S. Funahashi, J. Mol. Liq. **119**, 55 (2005).
[14] P. S. Salmon, M. C. Bellissent-Funel, and G. J. Herdman, J. Phys.: Condens. Matter **2**, 4297 (1990).
[15] B. M. Rode, C. F. Schwenk, and A. Tongraar, J. Mol. Liq. **110**, 105 (2004).
[16] T. H. Dunning, Jr., J. Chem. Phys. **53**, 2823 (1970).
[17] P. J. Hay and W. R. Wadt, J. Chem. Phys. **82**, 284 (1985).
[18] M. Pavlov, P. E. M. Siegbahn, and M. Sandström, J. Phys. Chem. A **102**, 219 (1998).
[19] S. Brode, H. Horn, M. Ehrig, D. Moldrup, J. E. Rice, and R. Ahlrichs, J. Comput. Chem. **14**, 1142 (1993).
[20] R. Ahlrichs, M. Bär, M. Häser, H. Horn, and C. Kölmel, Chem. Phys. Lett. **162**, 165 (1989).
[21] R. Ahlrichs and M. V. Arnim, *Methods and Techniques in Computational Chemistry: METECC-95* (STEF, Cagliari, 1995).
[22] M. V. Arnim and R. Ahlrichs, J. Comput. Chem. **19**, 1746 (1998).
[23] K. Kuchitsu, T. Morino, and M. Maeda, Bull. Chem. Soc. Jpn. **49**, 701 (1976).
[24] F. H. Stillinger and A. Rahman, J. Chem. Phys. **68**, 666 (1978).
[25] P. Bopp, G. Jansco, and K. Heinzinger, Chem. Phys. Lett. **98**, 129 (1983).
[26] G. Jansco, P. Bopp, and K. Heinzinger, Chem. Phys. **85**, 377 (1984).
[27] M. J. Elrod and R. J. Saykally, Chem. Rev. (Washington, D.C.) **94**, 1975 (1994).
[28] E. Clementi, H. Kistenmacher, W. Kolos, and S. Romano, Theor. Chim. Acta **55**, 257 (1980).
[29] L. A. Curtiss and R. Jurgens, J. Phys. Chem. **94**, 5509 (1990).
[30] L. A. Curtiss, J. W. Halley, J. Hautman, and A. Rahman, J. Chem. Phys. **86**, 2319 (1987).
[31] C. F. Schwenk, H. H. Loeffler, and B. M. Rode, J. Chem. Phys. **115**, 10808 (2001).
[32] J. I. Yagüe, A. M. Mohammed, H. H. Loeffler, and B. M. Rode, J. Phys. Chem. A **105**, 7646 (2001).
[33] T. Remsungnen and B. M. Rode, J. Phys. Chem. A **107**, 2324 (2003).
[34] H. J. Berendsen, J. R. Grigera, and T. P. Straatsma, J. Phys. Chem. **91**, 6269 (1987).
[35] M. P. Allen and D. J. Tildesley, *Computer Simulation of Liquids* (Oxford Science Publications, Oxford, 2003).
[36] D. J. Adams, E. M. Adams, and G. J. Hills, Mol. Phys. **38**, 387 (1979).
[37] P. Bopp, Chem. Phys. **106**, 205 (1986).
[38] S. H. Thomas, T. T. Hung, C. F. Schwenk, and B. M. Rode, J. Comput. Chem. **125**, 211 (2004).
[39] A. Musinu, G. Paschina, G. Piccaluga, and M. Magini, J. Appl. Crystallogr. **15**, 621 (1982).
[40] T. Radnai, G. Palinkas, and R. Caminiti, Z. Naturforsch. A **37**, 1247 (1982).
[41] T. Miyanaga, I. Watanabe, and S. Ikeda, Chem. Lett. **1988**, 1073.
[42] H. Sakane, T. Miyanaga, I. Watanabe, and Y. Yokoyama, Chem. Lett. **1990**, 1623.
[43] H. Ohtaki and T. Radnai, Chem. Rev. (Washington, D.C.) **93**, 1157 (1993).
[44] W. Bol, G. J. A. Gerrits, and C. L. van Panthaleon Eck, J. Appl. Crystallogr. **3**, 486 (1970).
[45] D. H. Powell, P. M. N. Gullidge, G. W. Neilson, and M. C. Bellissent-Funel, Mol. Phys. **71**, 1107 (1990).
[46] G. Licheri, G. Paschina, G. Piccaluga, and G. Pinna, Z. Naturforsch. A **37**, 1205 (1982).
[47] S. H. Thomas, B. R. Randolf, and B. M. Rode, Phys. Chem. Chem. Phys. **7**, 1382 (2005).
[48] W. B. Charles, A. K. Katz, and P. G. Jenny, J. Am. Chem. Soc. **117**, 3754 (1995).
[49] Y. P. Yongyai, S. Kokpol, and B. M. Rode, Chem. Phys. **156**, 403 (1991).
[50] A. P. Scott and L. Radom, J. Phys. Chem. **100**, 16502 (1996).
[51] D. J. DeFrees and A. D. McLean, J. Chem. Phys. **82**, 333 (1985).
[52] R. Armunanto, F. S. Christian, and B. M. Rode, J. Phys. Chem. A **107**, 3132 (2003).
[53] C. Kritayakornupong, K. Plankensteiner, and B. M. Rode, Chem. Phys. Lett. **371**, 438 (2003).
[54] T. Remsungnen and B. M. Rode, Chem. Phys. Lett. **367**, 586 (2003).
[55] B. M. Rode, C. F. Schwenk, T. S. Hofer, and B. R. Randolf, Coord. Chem. Rev. (to be published).
[56] D. Xenides, B. R. Randolf, and B. M. Rode, J. Chem. Phys. **122**, 174506 (2005).
[57] W. F. Murphy and H. J. Bernstein, J. Phys. Chem. **76**, 1147 (1972).
[58] D. Eisenberg and W. Kauzmann, *The Structure and Properties of Water* (Oxford University Press, Oxford, 1969).
[59] Y. Inada, H. H. Loeffler, and B. M. Rode, Chem. Phys. Lett. **358**, 449 (2002).
[60] H. Ohtaki and T. Radnai, Chem. Rev. (Washington, D.C.) **93**, 1157 (1993).